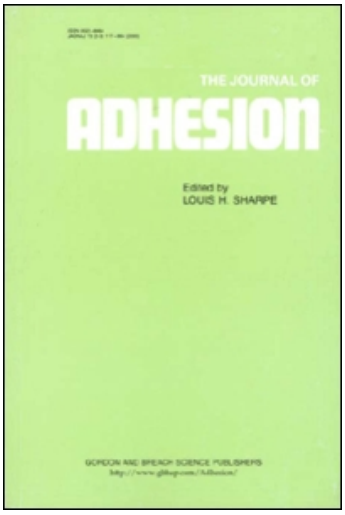

The Journal of Adhesion
Publication details, including instructions for authors and subscription information:
http://www.informaworld.com/smpp/title~content=t713453635

Temperature and Loading Rate Effects on the Fracture Behaviour of Adhesively Bonded GFRP Nylon-6,6

G. A. Wade[a]; W. J. Cantwell[a]
[a] Department of Engineering, University of Liverpool, Liverpool, UK

To cite this Article Wade, G. A. and Cantwell, W. J.(2001) 'Temperature and Loading Rate Effects on the Fracture Behaviour of Adhesively Bonded GFRP Nylon-6,6', The Journal of Adhesion, 76: 3, 245 — 264
To link to this Article: DOI: 10.1080/00218460108029628
URL: http://dx.doi.org/10.1080/00218460108029628

J. Adhesion, 2001, Vol. 76, pp. 245 - 264
Reprints available directly from the publisher
Photocopying permitted by license only

Temperature and Loading Rate Effects on the Fracture Behaviour of Adhesively Bonded GFRP Nylon-6,6

G. A. WADE* and W. J. CANTWELL

Department of Engineering, University of Liverpool, Liverpool L69 3GH UK

(Received 7 November 2000; In final form 3 March 2001)

The combined effect of varying test temperature and loading rate on the Mode II fracture toughness of plasma-treated GFRP Nylon-6,6 composites bonded using a silica-reinforced epoxy adhesive has been studied. End notch flexure tests have shown that the adhesive system used in this study offers a wide range of fracture energies that are extremely sensitive to changes in temperature and loading rate. Increasing the test temperature resulted in a substantial reduction in the Mode II fracture toughness of the adhesive, with the value of G_{IIc} at 60°C being approximately one-half of the room temperature value. In contrast, increasing the crosshead displacement rate at a given temperature has been shown to increase the value of G_{IIc} by up to 250%. Compression tests performed on bulk adhesive specimens revealed similar trends in the value of σ_y with temperature and loading rate. In addition, it was found that the plasma treatment employed in this study resulted in stable crack propagation through the adhesive layer under all testing conditions.

A more detailed understanding of the effect of varying temperature and loading rate on the failure mechanisms occurring at the crack tip was achieved using the double end notch flexure (DENF) geometry, which was considered in tandem with the fracture surface morphologies. Here, changes in the degree of matrix shear yielding and particle-matrix debonding were used to explain the trends in σ_y and G_{IIc}.

Keywords: Temperature; Loading rate; Silica-filled epoxy; Fracture energy; Yield stress; Failure mechanisms

*Corresponding author. Tel.: 0151 794 5391, Fax: 0151 794 4675, e-mail: swad@liv.ac.uk

INTRODUCTION

Fibre-reinforced thermoplastic composite systems are currently finding extensive use in a wide variety of load-bearing applications in the aerospace and automotive industries. Adhesive bonding is often used to join components, since this method can provide both superior three-dimensional stability and weight reductions compared with alternative joining methods such as mechanical fastening or welding. Epoxy-based structural adhesives have become an industry standard in the design and manufacture of load-bearing structures, and frequently include among the basic constituents a dispersed rubber phase or particulates for increased toughness and reduced production costs. Previous work has established that strong, durable bonds can be obtained using thermosetting adhesive systems between thermoplastic substrates, provided the latter are treated in some way prior to bonding [1, 2]. Exposure to a gas plasma is an accepted method for improving adhesion since this allows the composite surface to be modified in a controlled manner.

Much of the previously published work has focused on the effect of temperature and loading rate on the interlaminar fracture properties of thermoplastic composite systems and the bulk properties of polymers [3–7]. Similarly, many workers have characterised the sensitivity of reinforced epoxy systems to changes in temperature and loading rate [8–13]. However, few systematic attempts have been made to investigate the effect of these variables on the mechanical properties of adhesive joints. The aim of this work is to examine the effect of temperature and loading rate on the mechanical properties of adhesive joints based on glass fibre-reinforced Nylon substrates. No previous attempts of this type have been made with this material, despite its use in a number of important engineering applications.

EXPERIMENTAL PROCEDURE

Adhesive End Notch Flexure (ENF) Specimens

Unidirectional five-ply E-glass fibre-reinforced (GFRP) Nylon-6,6 laminates (approximately 1.7 mm thick) were prepared from a dry

prepreg using a hydraulic hot-press, under a pressure of 770 kPa. The 240 × 135 mm picture frame steel mould was lined with a fluorinated woven glass cloth to facilitate the removal of laminates following moulding. The average cooling rate over the range T_P (processing temperature, 290°C) − T_R (recrystallisation temperature, 230°C) was 85°C min^{-1}. Subsequent differential scanning calorimetry (10°C min^{-1} heating rate) and matrix burn-off testing (90 minutes at 650°C) showed the laminates contained a 20% crystalline volume fraction and 42% glass fibre by weight, respectively.

The moulded laminates were cut into 110 × 25 mm sections, with the fibres oriented in the longitudinal direction, and subsequently exposed to a capacitively-coupled, low-power (< 1 W) RF oxygen plasma. Previous work [2, 14] using this system has demonstrated that treatment in an oxygen plasma for 15 seconds or longer is generally sufficient to induce a change in failure mode from adhesive to cohesive when testing treated specimens bonded with a silica-filled epoxy adhesive. In the present study, the specimens were exposed to the oxygen plasma for 1 minute, which was considered to be a sufficiently long treatment time to ensure cohesive failure in the event that any given specimen(s) possessed an unusually high degree of contamination from the mould release agent.

Following plasma treatment, the specimens were immediately bonded using a two-component, silica-filled epoxy adhesive (Araldite 2015, Ciba-Geigy Ltd). End notch flexure (ENF) specimens were prepared by incorporating a folded piece of 25 μm thick aluminium foil at one end of the specimen, within the adhesive layer, to act as a starter defect (Fig. 1). The adhesive was cured at room temperature for 18 hours under a pressure of 85 kPa, resulting in an average bond thickness of approximately 120 μm. After bonding, the edges of

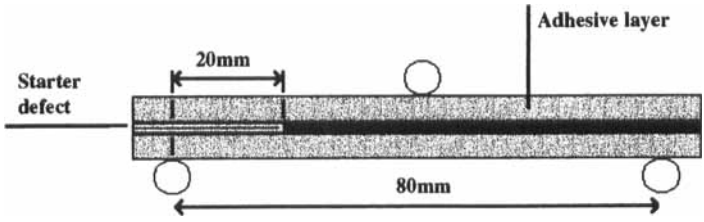

FIGURE 1 Adhesive Mode II End Notch Flexure (ENF) geometry.

specimens were ground using silicon carbide paper to remove any excess adhesive. Burn-off of the epoxy resin (3 hours at 650°C) revealed that the adhesive contained angular silica particles approximately 5 μm in size (2–10 μm range), although particles approaching 40 μm in size were occasionally observed. Other workers have shown that reinforcing particles of the order of 5 μm produce a considerably greater level of toughening compared with larger particles [15, 16].

The specimens were loaded in three-point bending (80 mm span) at constant crosshead displacement rates of 0.1, 10, and 500 mm·min^{-1} using a servoelectric tensile testing machine (Schenck Trebel). Test temperatures of 20, 40, and 60°C were achieved using an air-circulating oven fitted to the test machine. The relative humidity level in the laboratory was not controlled during testing, but was stable at approximately 50%. The specimens were left to soak at the required temperature for at least one hour prior to testing.

Following testing, the Mode II critical strain energy release rate, G_{IIc}, was calculated according to corrected beam theory [17], where

$$G_{IIc} = \frac{9P^2a^2}{16B^2Eh^3}, \tag{1}$$

where P is the maximum load at failure, a the initial crack length, B the specimen width, E the longitudinal elastic modulus of the bulk GFRP Nylon-6,6, and h the specimen half-thickness. A minimum of five specimens was tested for each condition in order to obtain mean values.

Compression Testing of the Bulk Adhesive

The rate and temperature sensitivity of the bulk adhesive was investigated through a series of uniaxial compression tests. This test method was employed since it is known that polymeric specimens generally fail in shear when loaded in compression [8].

Compression specimens were fabricated by allowing the adhesive system to cure at room temperature in rigid plastic tubes lined with a fluorinated woven glass cloth. The top and bottom faces of the specimens were then ground perpendicular to the gauge length with

the aid of an identical plastic tube mounted in epoxy resin. Finished specimens were cylindrical in shape with a cross-sectional area and gauge length of approximately 108 mm^2 and 22 mm, respectively (diameter to gauge ratio 0.52). The total void and silica contents were estimated at 2% and 25% by volume, respectively. The specimens were subsequently loaded in compression at constant crosshead displacement rates of 0.1, 10, and 500 $mm \cdot min^{-1}$, and at temperatures of 20, 40, and 60°C, as described previously. Since the composition (*i.e.*, silica and void contents) of the compression specimens was observed to be practically identical, only two specimens were tested for each condition.

The yield stress of the bulk adhesive was subsequently calculated at the knee of the load-displacement curve using a tangent construction, Figure 2a. This approach does not give the extrinsic yield stress defined by the Considère construction [8]; however, this analysis (Fig. 2b) could not be used as the engineering strain in the 45° shear plane of the compression specimens was unknown. However, a comparison of Figures 2a and 2b indicates it is likely that the load at the change of slope used to calculate the yield stress lies very near the extrinsic yield point. Thus, the yield stress determined in this study is

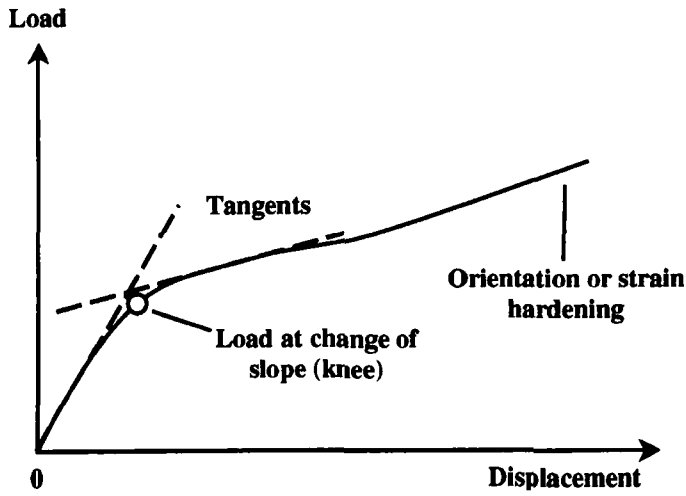

FIGURE 2a Determination of yield stress at the change of slope (knee) of the load-displacement curve as determined by tangent construction.

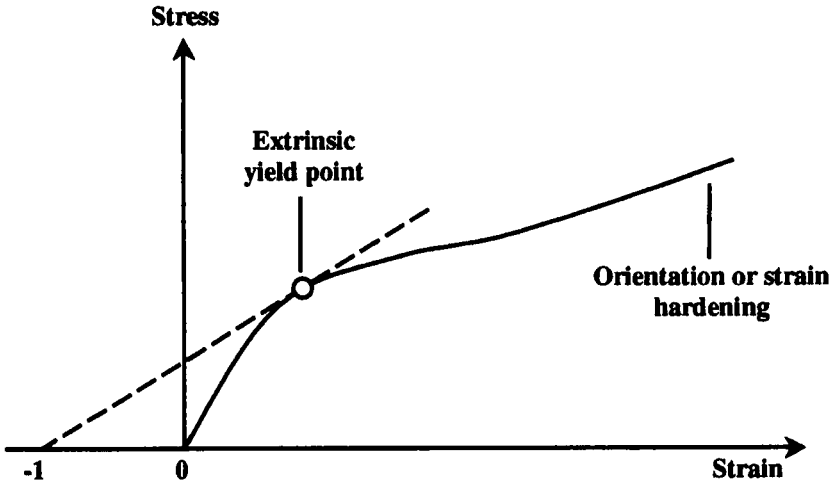

FIGURE 2b Determination of extrinsic yield stress according to the Considère construction (adapted from [8]).

similar to that which would have been obtained if the Considère construction were used.

Failure Mechanisms and Damage Characterisation

The fracture surfaces of adhesive ENF specimens tested at different temperatures and loading rates were investigated using scanning electron microscopy (SEM). Regions of interest were removed from the specimens and sputtered with silver (100 s in an Ar atmosphere) prior to analysis. The specimens were fixed to aluminium stubs, and electrically grounded with a thin layer of carbon dag (colloidal graphite). Images were obtained at an accelerating voltage of 25 kV (Hitachi S-2460N SEM).

The crack tip failure mechanisms were investigated using the adhesive double end notch flexure (DENF) geometry. This test essentially involved loading a three-point bend specimen containing identical starter defects at each end, and instantly unloading it following propagation of one of the defects, which was then termed the "primary" defect. The state of the crack tip plastic zone immediately before propagation was then investigated by examining the region surrounding the intact "secondary" defect at the other end

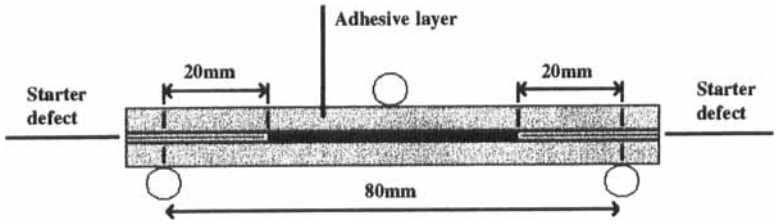

FIGURE 3 Adhesive Mode II Double End Notch Flexure (DENF) geometry.

of the specimen. Accordingly, specimens containing aluminium starter defects at both ends (Fig. 3) were prepared according to the manufacturing procedure outlined above. The specimen edges were then ground and polished to a 1 μm finish using a diamond-impregnated polishing cloth. In preparation for subsequent examination in the SEM, a thin layer of silver was sputtered onto one of the specimen edges. The specimens were loaded at 0.1 and 500 mm·mm^{-1} at 20 and 60°C, as described previously. However, for 20°C tests performed at 500 mm·mm^{-1} and all tests performed at 60°C, it was difficult to ensure that significant propagation of the secondary defect did not occur. At high loading rates this was mainly due to the inadequate response time of the instrumentation and/or operator, whereas at elevated temperatures the very low toughness of the adhesive rendered crack initiation difficult to judge. Therefore, these specimens were loaded approximately 1 mm off-centre (*i.e.*, with the specimen mid-span positioned 1 mm to the left or right of the centre of the loading point) to prevent any significant propagation of the secondary defect. Following testing, the specimens were examined in the SEM at an accelerating voltage of 10–12 kV, which minimised charging of the (uncoated) fracture surfaces created during testing. Photographs of both the ENF and DENF specimens were taken with the aid of a 35 mm camera assembly attached to the equipment.

RESULTS AND DISCUSSION

Figure 4 shows typical load-displacement curves for adhesive ENF tests performed at 20 and 60°C, and at crosshead displacement rates of

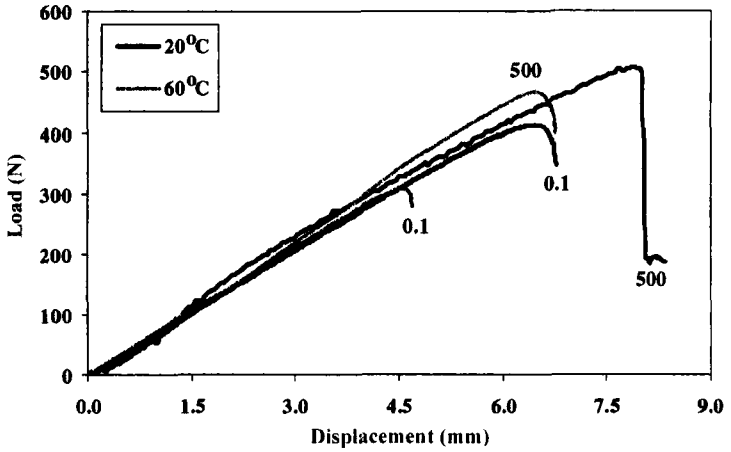

FIGURE 4 Typical ENF load-displacement traces at 20 and 60°C, and crosshead displacement rates of 0.1 and 500 mm·mm^{-1}.

0.1 and 500 mm·mm^{-1}. The curves are similar in appearance, although the maximum load and displacement clearly increases with decreasing temperature and/or increasing loading rate. It is also clear that the slopes of the curves are very similar, an observation that suggests that the flexural modulus is essentially insensitive to the variations in temperature and loading rate considered in this study. The specimens tested at 40°C (not shown here) also exhibited similar load-displacement behaviour.

The maximum load values obtained from the ENF tests were then used to determine the Mode II fracture toughness of this system (fracture energies were not calculated from DENF specimens). The combined effect of varying test temperature and crosshead displacement rate is shown in Figure 5. Here, it is clear that at a given temperature, the value of G_{IIc} increases significantly with increasing loading rate. Similar behaviour was observed by Hunston and Bascom following tapered double cantilever beam (TDCB) tests on aluminium substrates bonded using a rubber-modified epoxy adhesive [18]. It can also be seen that the slopes of the three trendlines in Figure 5 are very similar, which indicates that the relative increases in G_{IIc} with loading rate are also similar at a given temperature. The value of G_{IIc} varies (within the range of conditions

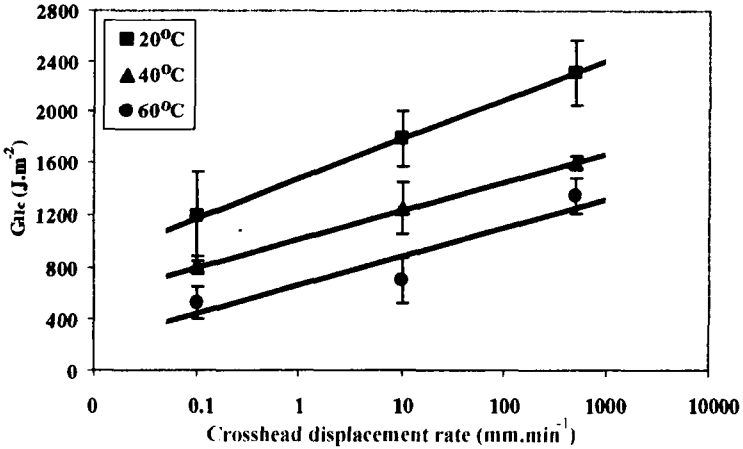

FIGURE 5 Variation of the Mode II fracture energy (G_{IIc}) with temperature and loading rate (error bars indicate one standard deviation).

considered in this study) from a minimum of $0.5\,kJ \cdot m^{-2}$ to a value of $2.3\,kJ \cdot m^{-2}$ at the lowest temperature and highest loading rate. Further testing (not presented here) has shown that the value of G_{IIc} may be as high as $4.3\,kJ \cdot m^{-2}$ when loaded under low-velocity impact conditions at 20°C.

In order to further investigate the temperature-rate dependency of the adhesive ENF specimens, a number of tests were undertaken in which the crosshead displacement rate was increased by an order of magnitude at the moment at which the force reached a plateau in the load-displacement curve. The upper part of such a curve for an adhesive ENF specimen loaded at 20°C is shown in Figure 6. The initial crosshead displacement rate during this test was $0.1\,mm \cdot mm^{-1}$, and the force peaked at a value of 420 N. At this point, the crosshead displacement rate was increased to $1.1\,mm \cdot mm^{-1}$ and the force peaked at 450 N after a short period of linear behaviour. Finally, a crosshead displacement rate of $11.1\,mm \cdot mm^{-1}$ was employed and the force peaked at 475 N. The same behaviour was observed (at correspondingly lower loads) for specimens tested at 40 and 60°C. This evidence clearly highlights a viscoelastic response and substantiates the data presented in Figure 5. Similar behaviour was observed by Berger and Cantwell following ENF tests on unidirectional carbon fibre reinforced PEEK [3].

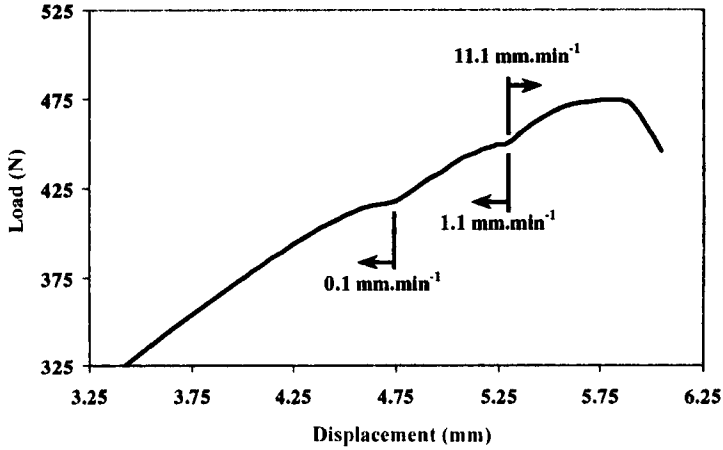

FIGURE 6 Load-displacement curve for an ENF specimen loaded at 20°C in which the crosshead displacement rate was sequentially increased at each force plateau.

An inspection of the edges of the adhesive ENF specimens during and after testing established that the failure mode was invariably cohesive within the adhesive layer. This evidence suggests that the results shown in Figure 5 can be attributed to the properties of the adhesive system. Since crack propagation was constrained entirely within the adhesive layer, the GFRP Nylon-6,6 composite laminates appear to have behaved merely as reinforcing substrates. Thus, the fracture behaviour of the specimens can be interpreted in terms of the temperature-rate properties of the adhesive system alone.

Figure 7 shows the combined effect of temperature and loading rate on the compression yield stress of the bulk epoxy adhesive. The influence of voids (2% by volume) was considered to be negligible [9]. It is clear that the yield behaviour of the adhesive in compression (where failure occurs in shear) is remarkably similar to that of the adhesive ENF specimens, which supports the assumption that the trends reported above are due to the temperature-rate sensitivity of the adhesive system. In a manner similar to that illustrated in Figure 5, the slopes of the three trendlines in Figure 7 are very similar, indicating that the relative increases in yield stress with loading rate are also similar at a given temperature. It is interesting to note that the data presented in Figures 5 and 7 exhibit similar trends to those observed

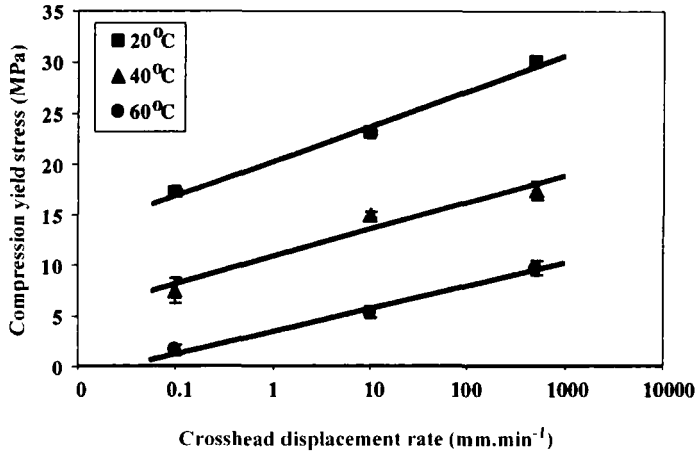

FIGURE 7 Variation of the compressive yield stress (σ_y) with temperature and loading rate (error bars indicate one standard deviation).

by Bauwens-Crowet *et al.* following tensile tests on polycarbonate samples, where plots of σ_y/T (yield stress/test temperature) against log (strain rate) gave a series of parallel lines at different temperatures [5]. This correlation further highlights the relationships between G_{IIc}, σ_y, and temperature obtained in this study. It should be noted that the strain rate at the crack tip of an ENF specimen loaded at a given crosshead displacement rate is not necessarily the same as that obtained in compression at the same rate. However, an order of magnitude change in loading rate is likely to produce an order of magnitude change in the strain rate in both ENF and compression specimens. Hence, the values of G_{IIc} and σ_y may be qualitatively related. Figure 8 shows the relationship between the adhesive Mode II fracture energy and the yield stress of the adhesive system, where it is apparent that the value of G_{IIc} increases linearly with increasing yield stress.

It is interesting to observe that the adhesive exhibited pronounced viscoelastic behaviour in both types of test despite having been loaded below the glass transition temperature of the epoxy resin matrix. Similar observations have been reported by other workers [10–11, 19]. Since the specimens were bonded at room temperature, the degree of crosslinking in the cured adhesive system is likely to be relatively low.

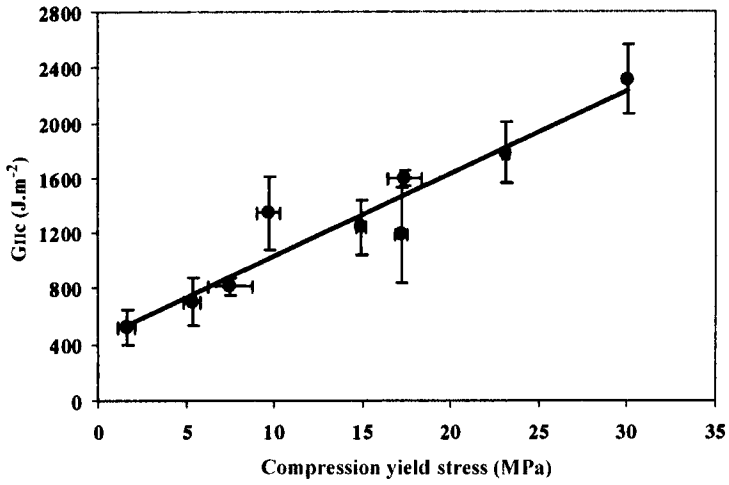

FIGURE 8 Relationship between G_{IIc} and σ_y for all temperatures and loading rates (error bars indicate one standard deviation).

This would increase the toughness of the adhesive and may also result in enhanced viscoelastic behaviour at temperatures below the glass transition temperature. These aspects are supported by the observation that the maximum compression yield stress obtained in this study (30 MPa; 20°C, 500 mm·mm^{-1}) is significantly lower than similar particle-reinforced systems (130 MPa; 20% silica-filled epoxy [20]) processed at higher temperatures, which are, therefore, likely to possess a greater degree of crosslinking and a higher glass transition temperature. Also, Sharon *et al.* [11] have reported yield stresses similar to those obtained in this study using room temperature curing epoxy systems.

Figures 9a to 9d show the fracture surface morphologies of adhesive ENF specimens tested at 20 and 60°C, and at crosshead displacement rates of 0.1 and 500 mm·mm^{-1}. Figure 9a (60°C, 0.1 mm·mm^{-1}), highlights the extent of plastic flow and particle-matrix debonding prevalent in the adhesive system at very low yield stresses. Significant ductile tearing of the matrix is evident in the region immediately below the debonded silica particle, which remained intact despite its large size. The fracture surface of this specimen exhibited a considerable degree of particle-matrix debonding and matrix plastic flow, and this micrograph is typical of the fracture surface as a whole. Figure 9b

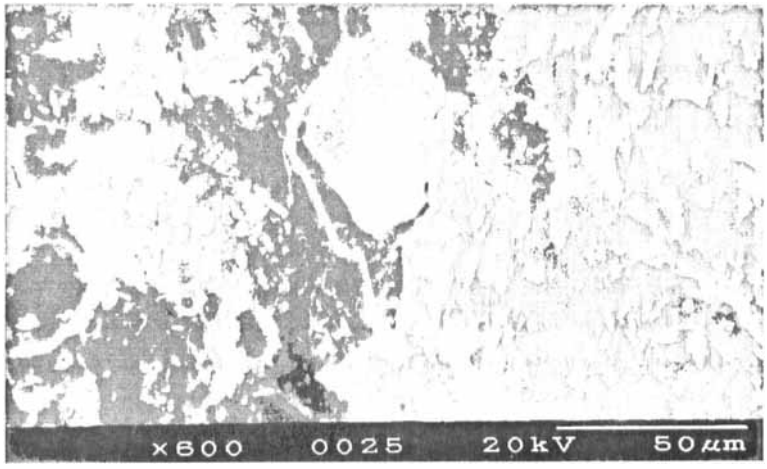

FIGURE 9a SEM fracture surface (60°C, 0.1 mm·mm $^{-1}$) showing extensive particle-matrix debonding and matrix ductile tearing.

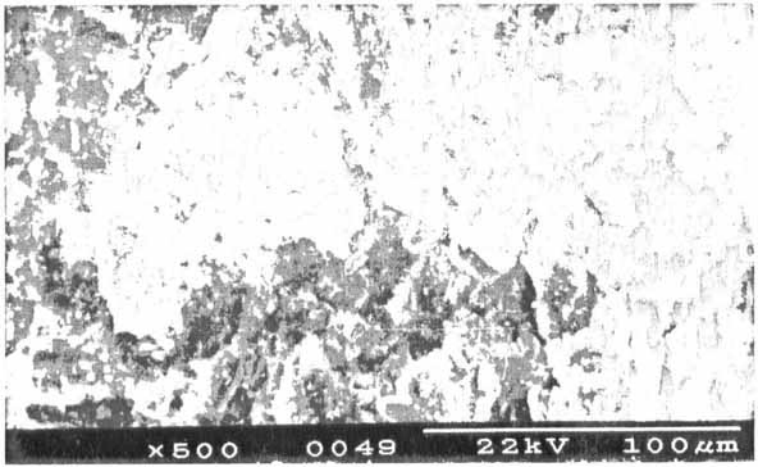

FIGURE 9b SEM fracture surface (60°C, 500 mm·mm $^{-1}$) showing regions of brittle failure combined with matrix ductile tearing.

(60°C, 500 mm·mm^{-1}) appears to exhibit features characteristic of both ductile and brittle behaviour. The left of this figure highlights a region of adhesive that has fractured in a brittle manner; however, plastic flow is also present in the centre of the figure, where a ductile

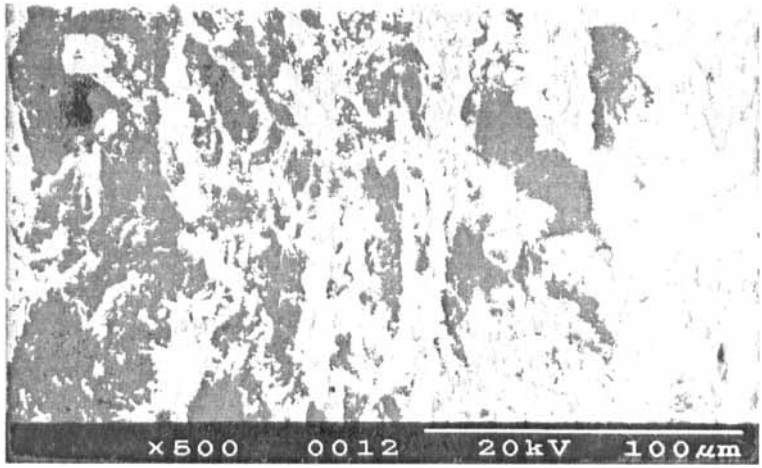

FIGURE 9c SEM fracture surface (20°C, 0.1 mm·mm $^{-1}$) showing little evidence of particle-matrix debonding or matrix plastic flow.

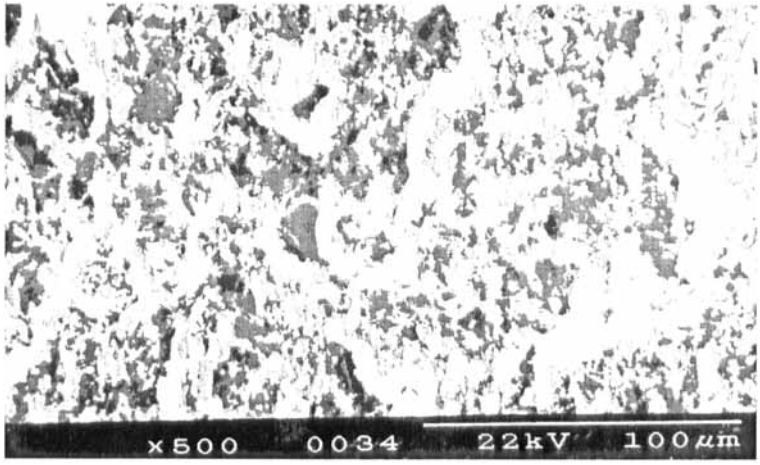

FIGURE 9d SEM fracture surface (20°C, 500 mm·mm $^{-1}$) showing highly planar, brittle morphology.

tear can be seen extending upwards. Little evidence of plastic flow or debonding is apparent on the fracture surface of specimens loaded at 20°C, 0.1 mm·mm^{-1} (Fig. 9c), although the slightly fibrous nature of this surface suggests that limited ductility is present. It was also

observed that the fracture surfaces presented in Figures 9b and 9c were generally very similar, which is unsurprising given that the values of G_{IIc} and σ_y were approximately equal for these two conditions. Figure 9d (20°C, 500 mm·mm^{-1}) presents a highly planar, brittle topography, with no evidence of plastic flow or particle-matrix debonding.

In general, it was observed that the extent of plastic flow and particle-matrix debonding decreased as the temperature was decreased and/or the crosshead displacement rate was increased (*i.e.*, the yield stress of the material was increased). The reasons for this will be discussed shortly. The micrographs shown in Figure 9, though informative, only show completely fractured surfaces and, therefore, not provide information regarding the mechanisms leading to failure at the crack tip. In an attempt to further characterise the deformation and failure mechanisms in the epoxy adhesive system, the adhesive DENF geometry was employed as described earlier. The SEM micrographs obtained from these specimens are shown in Figures 10a to 10d.

Examination of adhesive DENF specimens at the lowest crosshead displacement rate (and therefore low σ_y) highlighted the presence of extensive particle-matrix debonding and microcracking (Fig. 10a).

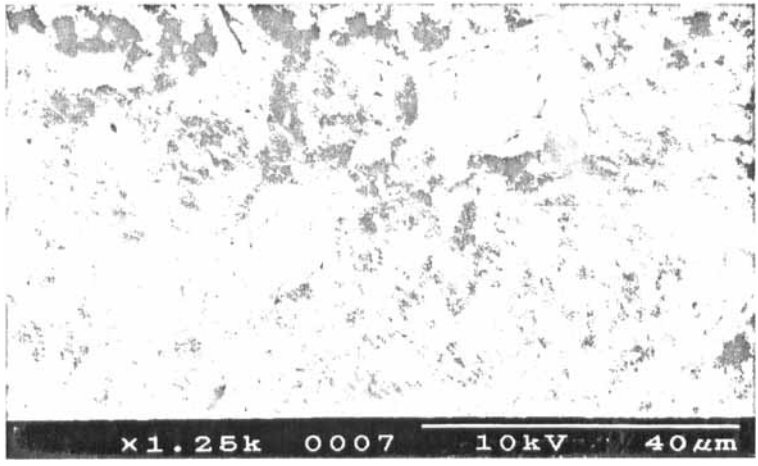

FIGURE 10a DENF micrograph (60°C, 0.1 mm·mm^{-1}) showing extensive particle-matrix debonding and matrix shear yielding.

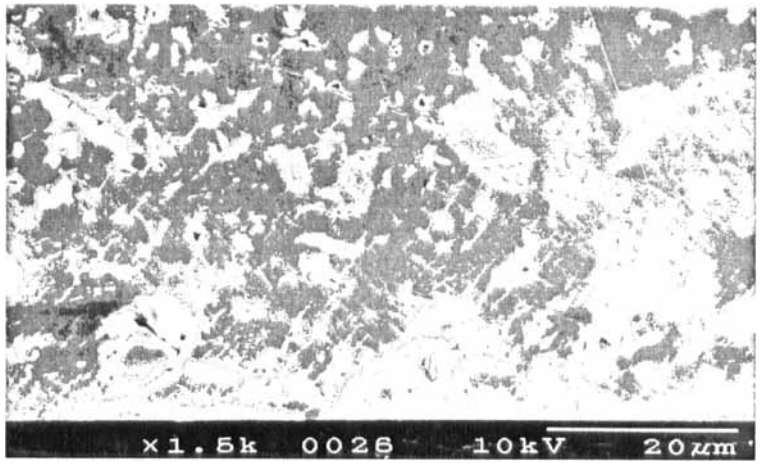

FIGURE 10b DENF micrograph (60°C, 500 mm·mm^{-1}) showing moderate particle-matrix debonding and matrix shear yielding.

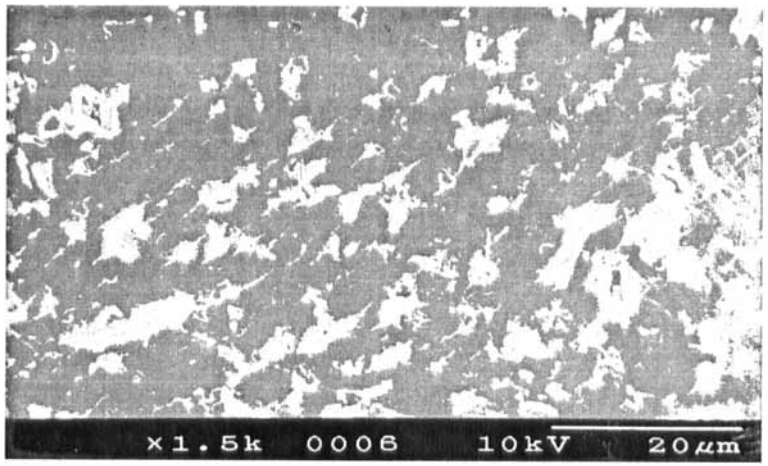

FIGURE 10c DENF micrograph (20°C, 0.1 mm·mm^{-1}) showing moderate particle-matrix debonding and matrix shear yielding.

Closer inspection revealed that the microcracks were features present only in the sputtered metallic layer, which indicates that extensive shear yielding of the epoxy matrix had occurred [3]. Many of the microcracks were observed to be oriented at approximately 45° to

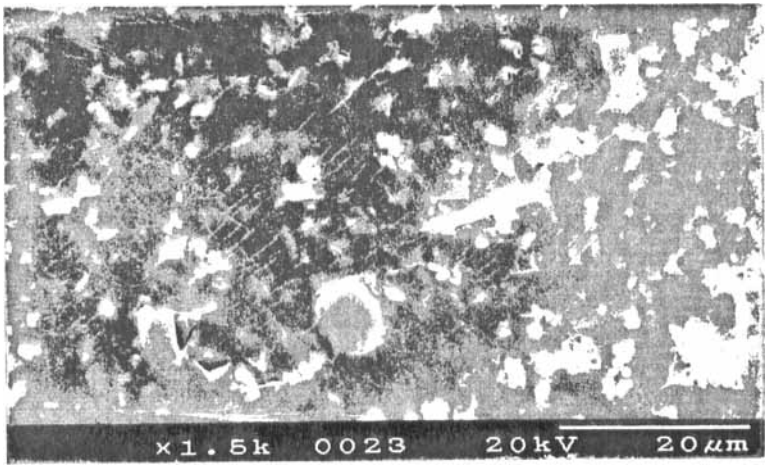

FIGURE 10d DENF micrograph (20°C, 500 mm·mm $^{-1}$) showing slight particle-matrix debonding and matrix shear yielding.

the longitudinal axis of the specimen, as expected since tensile stresses are greatest in this direction. It was observed that virtually every silica particle in the failed adhesive layer was debonded from the matrix, irrespective of its size or shape. This would give rise to a significant amount of additional shear yielding associated with the free surfaces created around debonded particles. The debonded silica particles are no longer capable of effectively reinforcing the adhesive or resisting crack propagation and effectively act as voids which occupy a significant proportion of the adhesive layer. Eventually, the integrity of the material is reduced so severely by debonding and shear yielding that it can no longer support increased loading, and as a result failure occurs at very low loads with correspondingly low values of G_{IIc}.

As the crosshead displacement rate was increased, the extent of particle-matrix debonding and shear yielding was generally observed to decrease. It was seen that the degree of damage present in specimens tested at 60°C, 500 mm·mm^{-1} (Fig. 10b) and 20°C, 0.1 mm·mm^{-1} (Fig. 10c) were very similar, which is unsurprising given that the values of G_{IIc} and σ_y were very similar for these two conditions, as were the fracture surfaces. This is because, for viscoelastic solids, temperature and loading rate are interrelated in

terms of controlling yield behaviour. That is, increasing the test temperature can be considered equivalent to decreasing the loading rate, and *vice-versa*.

An analysis of adhesive DENF specimens at the highest crosshead displacement rate highlighted only small quantities of particle-matrix debonding and shear yielding (Fig. 10d). Furthermore, deformation appeared to be confined to the immediate area surrounding the propagated crack, with the majority of the adhesive layer remaining undeformed. This is significantly different from the behaviour observed at lower loading rates, where damage had occurred over a considerable distance ahead of the crack tip. It is likely that the extent of particle-matrix debonding and shear yielding was slight at high crosshead displacement rates because the matrix was too rigid to allow sufficient plastic flow in the matrix and around the particles for shear flow or debonding to initiate. In addition, it was observed that only the larger silica particles (relative to the thickness of the adhesive layer) suffered debonding, due to the subjection of these particles to different (higher) stress conditions compared with smaller particles; the majority of which remained intact and well bonded to the matrix material. In this state, the damage sustained by the specimen during loading is minimal, the silica particles can continue to reinforce the adhesive effectively and, as a result, the resistance of the material to crack initiation is excellent. In such circumstances, complete failure of the specimen can initiate from a single debonding event [12]. Following the initial debonding process, the crack accelerates rapidly and propagates predominantly through the matrix, as shown in Figure 9d.

In summary, the value of G_{IIc} of a bonded joint appears to be directly related to the material's ability to resist shear flow at the crack tip. If the yield stress of the adhesive is very low, it will flow easily at the crack tip, offering little resistance to crack initiation. This is further compounded by the fact that this excessive shear flow triggers debonding and additional shear yielding. These damage mechanisms will clearly reduce the integrity of the material and its resistance to crack propagation. Conversely, if the crosshead displacement rate is higher, the adhesive has a greater resistance to shear failure and subsequent debonding; consequently, the measured value of G_{IIc} is much greater. The proposed dependency of G_{IIc} on the yield stress is

supported by the load-displacement curve shown in Figure 6 and the data shown in Figure 8.

CONCLUSIONS

A series of Mode II fracture tests have been conducted on plasma-treated GFRP Nylon-6,6 composites bonded using a silica reinforced epoxy adhesive. Tests have shown that the Mode II fracture toughness decreases with increasing temperature and increases with increasing loading rate. The failure mode was observed to be cohesive through the adhesive under all conditions. Compression testing of the bulk adhesive system under the same range of conditions demonstrated that the Mode II fracture energy of the adhesive system is related to the yield stress of the adhesive. The crack tip failure mechanisms have been elucidated using the adhesive DENF geometry in conjunction with the ENF fracture surface morphology, where matrix shear yielding and particle-matrix debonding were identified as the main damage mechanisms that control failure.

The findings suggest that the Mode II fracture energy of this adhesive is likely to be even lower at crosshead displacement rates below those considered here, suggesting that its response to long-term loading conditions could be a source for concern. It should be noted, however, that almost all operational joints are likely to be subjected to a mixed-mode type of loading; thus, the effect of loading rate on the mixed-mode fracture properties of the adhesive should be investigated.

Acknowledgement

G. A. Wade gratefully acknowledges the financial support of the Engineering and Physical Sciences Research Council (EPSRC); award number 9832095X.

References

[1] Kodokian, G. K. A. and Kinloch, A. J., *J. Adhesion* **29**, 193 (1989).
[2] Wade, G. A., Cantwell, W. J. and Pond, R. C., *Interface Sci.* **8**, 363 (2000).
[3] Berger, L. and Cantwell, W. J., *Poly. Comp.* (to be published).
[4] Mall, S., Law, G. E. and Katouzian, M., *J. Comp. Mats* **21**, 569 (1987).

[5] Bauwens-Crowet, C., Bauwens, J. C. and Homes, G., *J. Poly. Sci.: Pt. A-2* **7**, 735 (1969).
[6] Frassine, R., Rink, M. and Pavan, A., *Comp. Sci. Tech.* **56**, 1253 (1996).
[7] Chapman, T. J., Smiley, A. J. and Pipes, R. B., *Proc. ICCM6/ECCM2*, Matthews, F. L., Buskell, N. C. R., Hodgkinson, J. M. and Morton, J., Eds. **3**, 295 (1987).
[8] Kinloch, A. J. and Young, R. J., *Fracture Behaviour of Polymers* (Applied Science Publishers, London, 1983), Chap. 4.
[9] Mouritz, A. P. and Hutchings, I. M., *J. Mat. Sci. Letters* **11**, 1100 (1992).
[10] McMurray, M. K. and Amagi, S., *J. Comp. Mats.* **32**, 1836 (1998).
[11] Sharon, G., Dodiuk, H. and Kenig, S., *J. Adhesion* **31**, 21 (1989).
[12] Smith, J. W., Cantwell, W. J., Demarmels, A. and Kausch, H. H., *J. Mat. Sci.* **26**, 5534 (1991).
[13] Smith, J. W., Kaiser, T. and Roulin-Moloney, A. C., *J. Mat. Sci.* **23**, 3833 (1988).
[14] Wade, G. A. and Cantwell, W. J., *J. Mat. Sci. Letters* **19**, 1829 (2000).
[15] Nakamura, Y., Yamaguchi, M., Okubo, M. and Matsumoto, T., *Polymer* **32**, 2976 (1991).
[16] Nakamura, Y., Okabe, S. and Iida, T., *Polymers and Polymer Composites* **7**, 177 (1999).
[17] Davies, P., *Protocols for Interlaminar Fracture Testing*, European Structural Integrity Society, IFREMER (1993).
[18] Hunston, D. L. and Bascom, W. D., *Amer. Chem. Soc.: Adv. in Chem. Series* (*conf. code 06960*), **83** (1984).
[19] Koh, S.-W., Kim, J.-K. and Mai, Y. W., *Polymer* **34**, 3446 (1993).
[20] Moloney, A. C., Kausch, H. H., Kaiser, T. and Beer, H. R., *J. Mat. Sci.* **22**, 381 (1987).